Inorganic Chemistry

Article

pubs.acs.org/IC

Synthesis and Structural and Electrical Investigations of a Hexagonal $Y_{1-x}Gd_xInO_3$ ($0.0 \leq x \leq 1.0$) System Obtained via Metastable C-Type Intermediates

Rakesh Shukla,[†] Vinita Grover,*[,†] S. K. Deshpande,[‡] Dheeraj Jain,[†] and Avesh K. Tyagi*[,†]

[†]Chemistry Division and [‡]UGC-DAE Consortium for Scientific Research, Bhabha Atomic Research Centre Mumbai 400085, India

Supporting Information

ABSTRACT: Detailed structural and electrical investigations were carried out on an A-site disordered hexagonal $Y_{1-x}Gd_xInO_3$ ($0.0 \leq x \leq 1.0$) series synthesized by a self-assisted gel-combustion route. The phase relations show profound temperature dependence. The metastable C-type modification could be stabilized for all the compositions, which on further heating get converted to stable hexagonal polymorphs. The conversion temperature (C-type to hexagonal) was found to increase with an increase in Y^{3+} content. The system was observed to be single-phasic hexagonal at 1250 °C throughout the composition range. Interestingly, the increase in planar bonds of InO_5 polyhedra was found to be twice that of the apical bonds on Gd^{3+} substitution. Careful Raman spectroscopic studies highlighted a definitive though subtle structural change from $x = 0.7$ onward. The same observation is also corroborated by the dielectric studies. Electric field-dependent polarization measurements showed the ferroelectric hysteresis loop for pure $YInO_3$. The system transforms from ferroelectric in $YInO_3$ to almost paraelectric for $GdInO_3$. In the present study, XRD, Raman, and electrical characterizations in conjunction reveal that to tune the electrical properties of the hexagonal rare earth indates, the variation in tilting of InO_5 polyhedra has to be influenced, which could not be brought about by isovalent A-site substitution.

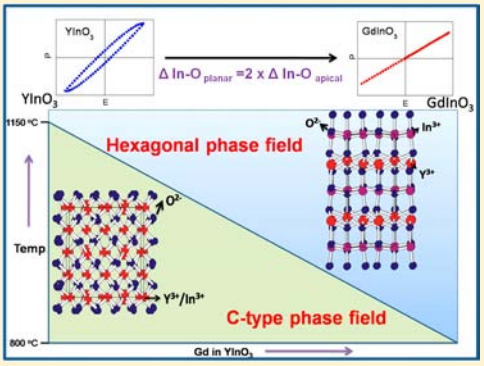

INTRODUCTION

The compounds with the nominal formula ABO_3 are most generally synonymous with the perovskite lattice. However, as described by Giaquinta et al.,[1] the ABO_3 composition can adopt a variety of interesting structures such as corundum, bixbyite, ilmenite, perovskites, and several interesting hexagonal phases depending on various factors, of which the most important is relative radius of the A-site and the B-site cations. It has been found that if the Goldschmidt's tolerance factor, t (given by $(r_A + r_O)/\sqrt{2}(r_B + r_O)$, is 1, it would result in an ideal perovskite structure. However, if the A-cation is smaller than what is required to form an ideal perovskite structure, the BO_6 octahedra tilt, resulting in the lower symmetry orthorhombic structure. A further decrease in tolerance factor subsequently leads to the formation of hexagonal structures (space group $P6_3cm$ and $P6_3mmc$) wherein the A-cation has 7-fold coordination and the B-cations are situated in the 5-fold trigonal bipyramidal sites. This hexagonal structure in only known for trivalent A cations, which may be In or a small rare-earth ions (Gd–Lu, Sc). It is reported that the B cation can be Al, Ga, In, Mn, Fe, 1:1 Cu/Ti, 2:1 Cu/V, or 3:1 Cu/Mo.[2−8] Hexagonal $AMnO_3$ compounds have been of interest as multiferroics because these compounds are ferroelectric and magnetically ordered.[9]

Rare earth indates (RE = Eu–Ho, Y), which can be prepared at atmospheric pressure, crystallize in a hexagonal ($a \approx 6.3$ Å, $c \approx 12.3$ Å, $Z = 6$) $LuMnO_3$-type lattice and possess the non-centrosymmetric space group $P6_3cm$.[10] Structurally rare-earth indates are intriguing because it is not very common for In^{3+} to occupy trigonal bipyramidal (TBP) coordination, unlike Mn^{3+}. Rare-earth indates, $REInO_3$, as well other compounds belonging to the hexagonal ABO_3 structure, have evoked a lot of interest in recent years owing to the possibility of the existence of geometric ferroelectricity in these materials.[11] This has been attributed to the non-centrosymmetric atomic arrangement of the crystal caused merely by the relative ionic size effect, which does not depend upon d^0 (Nb, Ta) or the lone-pair ions (Bi^{3+}, Pb^{2+}) like the conventional dielectrics. The hexagonal indates are known to exist in both paraelectric (space group: $P6_3mmc$) and ferroelectric forms (space group: $P6_3cm$), and the transition between these two is displacive in nature. It has been found that ferroelectricity on these compounds is the interplay of bending of the BO_5 trigonal bipyramid and the different A–O bond lengths along the c-axis.[12] Both these factors can be controlled by suitable substitution at RE- and In-sites of $REInO_3$. In our previous study on $GdIn_{1-x}Sc_xO_3$, substituting Sc at the In-site could bring about interesting structural changes in the system, which has a direct manifestation on the electrical behavior of the system, wherein the composition $GdIn_{0.9}Sc_{0.1}O_3$ depicted relaxor behavior. In fact,

Received: August 14, 2013
Published: November 6, 2013

   dx.doi.org/10.1021/ic402085w | Inorg. Chem. 2013, 52, 13179–13187

due to the property being controlled primarily by the structure adopted by ABO_3 compositions, this class forms an interesting case study for studying the structure−electrical property correlation. This also becomes important in wake of the fact that this mechanism offers a new route for designing magnetic-ferroelectrics that have been historically difficult to achieve, but are appealing for "spintronics" applications.[9]

There have been few studies that have explored the substitution of hexagonal $YInO_3$ from the point of view of developing a new color pigment.[13] However, these studies explore the substitution at the In-site (B-site), and also the variation in electrical behavior subsequent to the substitution has also not been investigated. In view of this, the present study attempts to explore the variation in structure and electrical properties brought about by the Gd^{3+} substitution in hexagonal $YInO_3$. The various compositions are thoroughly characterized by X-ray diffraction (XRD), Raman spectroscopy, and ac impedance spectroscopy. It has been attempted to correlate the structural evolution in the $Y_{1-x}Gd_xInO_3$ ($0.0 \le x \le 1.0$) series with the evolution of electrical behavior.

EXPERIMENTAL SECTION

Analytical reagent grade powders of Gd_2O_3, Y_2O_3, In_2O_3, and glycine were used as the starting reagents. The various nominal compositions were synthesized by the self-propagating gel combustion method. Herein, to obtain different compositions of $Y_{1-x}Gd_xInO_3$ ($0.0 \le x \le 1.0$), stoichiometric amounts of reactants were dissolved as nitrates and were made to undergo combustion in the presence of glycine as fuel. The combustion reactions were carried out in the fuel-deficient stoichiometry wherein oxidant-to-fuel (O/F) was kept at 1:1.5 (stoichiometric O/F ratio for this reaction is 1:3.33). The combustion proceeds at acidic pH, and no special efforts were made to control the pH in the present study. The solutions were dehydrated to highly viscous liquids (gels). At this stage, the temperature was raised to 250 °C. The viscous liquid then swelled and autoignited, with a rapid evolution of a large volume of gases. This resulted in fine powders with large surface area. The powders were calcined at 600 °C and then heated at several temperatures from 850 to 1250 °C in static air to obtain the products.

CHARACTERIZATION

The products were characterized by powder X-ray diffraction using monochromatized Cu Kα radiation on a Panalytical Xpert Pro. Silicon was used as external standard. The patterns were refined using the refinement program Fullprof 2000.[14]

Raman spectroscopic measurements were carried out on a micro/macro-Raman spectrometer (LABRAM-1, France) using the 488 nm line of an Ar^+ ion laser for excitation. The scattered Raman signal was collected using a single-monochromator spectrometer equipped with a Peltier-cooled CCD detector in the backscattering geometry. Samples were used in the form of pellets, and the laser line was focused on a flat surface of the sample using an optical microscope (Olympus BX-40, 50× objective lens) connected to the spectrometer. The spectra recorded were averaged out of 50 scans with a time interval of 2 s and a resolution of 2 cm^{-1}.

The electric field dependent polarization (PE studies) were performed using an Aixacct TF Analyzer 2000. The analysis was done by performing measurements at a range of frequencies and voltages. The dielectric properties of the $Y_{1-x}Gd_xInO_3$ compounds were measured over a temperature range from 30 to 300 °C and a frequency range of 100 Hz to 5 MHz using a Novocontrol Alpha-AN impedance analyzer (Novocontrol Technologies GmbH, Germany) equipped with a Quatro nitrogen gas cooling/heating system. Samples in the form of cylindrical pellets were sandwiched between two gold-plated electrodes in a parallel plate capacitor configuration. Samples were coated with silver paste for proper electrical contact.

RESULTS AND DISCUSSION

The $Y_{1-x}Gd_xInO_3$ ($0.0 \le x \le 1.0$) system was synthesized by a self-assisted gel combustion route followed by calcination at 600 °C. The XRD patterns of the calcined powders (Figure 1a)

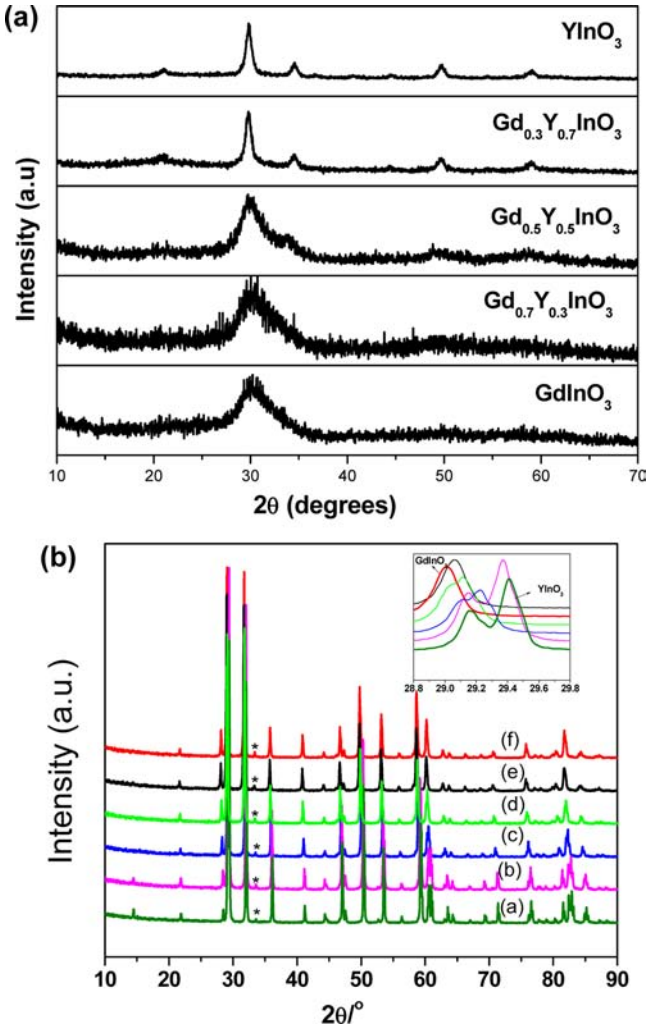

Figure 1. (a) XRD of the as-prepared sample after calcination in air at 600 °C. (b) XRD of $Y_{1-x}Gd_xInO_3$ after heating in air at 1250 °C, where x is (a) 0.0, (b) 0.1, (c) 0.5, (d) 0.7, (e) 0.9, (f) 1.0.

revealed that all the nominal compositions possess a C-type structure ($Ia\bar{3}$) with the peaks getting broader with an increase in the amount of Gd^{3+}. The C-type or the bixbyite structure is related to the F-type (fluorite structure) and is derived from the fluorite lattice by removal of one-quarter of the anions and subsequent rearrangements. Consequently, two types of cation arrangements are generated, which have six neighbors (instead of eight in the fluorite structure) at the vertices of the cube. For one kind of cation, two anions are missing at the ends of the face diagonal, and for the other the anions are missing at the end of the face diagonal. The X-ray peak broadening in Figure 1a has been analyzed for particle size and strain variation across the series. It is observed that the particle size decreases

dx.doi.org/10.1021/ic402085w | Inorg. Chem. 2013, 52, 13179−13187

Table 1. Crystallographic Data, Tolerance Factor, and Structure Refinement Parameters of the $Y_{1-x}Gd_xInO_3$ ($0.0 \le x \le 1.0$) System

molecular formula	GdInO3	$Gd_{0.9}Y_{0.1}InO_3$	$Gd_{0.7}Y_{0.3}InO_3$	$Gd_{0.5}Y_{0.5}InO_3$	$Gd_{0.3}Y_{0.7}InO_3$	$Gd_{0.1}Y_{0.9}InO_3$	$YInO_3$
MW	320.07	313.24	299.57	285.90	272.23	258.56	251.72
tolerance factor	0.8445	0.8425	0.8397	0.8370	0.8344	0.8309	0.8295
space group	$P6_3cm$	$P6_3cm$	$P6_3cm$	$P6_3cm$	$P6_3cm$	$P6_3cm$	$P\ 6_3cm$
unit cell params							
a (Å)	6.3472(1)	6.3479(8)	6.3308(7)	6.3131(9)	6.2972(1)	6.2812(1)	6.2727(1)
b (Å)	6.3472(1)	6.3479(8)	6.3308(7)	6.3131(9)	6.2972(1)	6.2812(1)	6.2727(1)
c (Å)	12.3400(2)	12.3176(4)	12.3096(4)	12.2867(5)	12.2731(4)	12.2631(1)	12.2563(0)
vol (Å^3)	430.54(2)	429.86(2)	427.27(1)	424.09(7)	421.48(1)	419.00(2)	417.63(9)
no. of params	10	10	10	10	10	10	10
refinement	Rietveld refinements (Fullprof-2K) (Rodriguez-Caravjal, 2000)						
profile	Pseudovoigt						
goodness-of-fit (χ^2)	2.43	2.46	1.64	2.01	2.25	2.22	1.73
R_P	8.63	14.0	11.9	12.2	12.3	11.3	10.6
R_{wp}	11.6	21.6	17.0	18.9	18.3	16.0	15.3
R_F	9.43	8.8	7.66	7.48	8.57	4.81	5.56

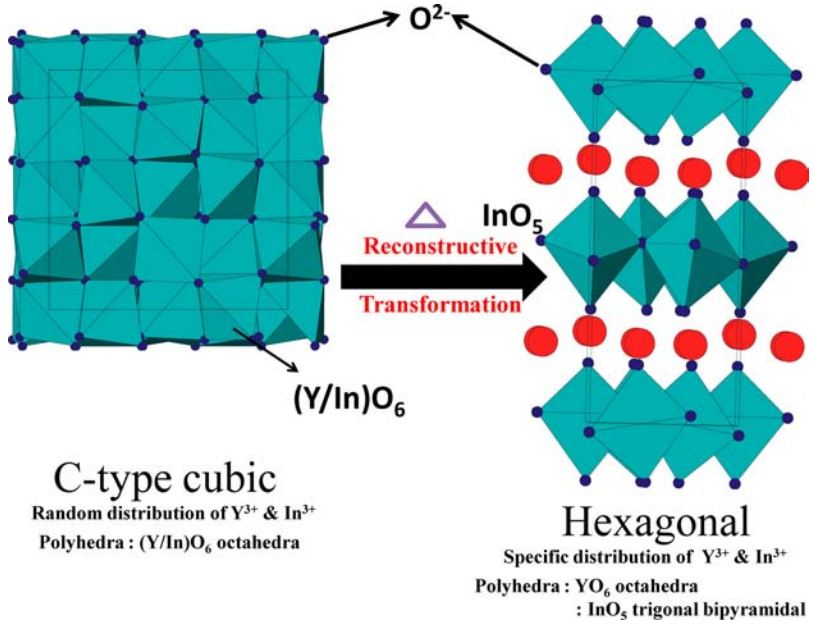

Figure 2. Representation of the structure of $YInO_3$ in C-type cubic form and hexagonal perovskite related form.

Table 2. Phases Observed in the $Y_{1-x}Gd_xInO_3$ ($0.0 \le x \le 1.0$) System at Various Temperatures

composition	as-prepared (600 °C)	800 °C	850 °C	900 °C	1000 °C	1250 °C
$GdInO_3$	C-type	hexagonal	hexagonal	hexagonal	hexagonal	hexagonal
$Y_{0.1}Gd_{0.9}InO_3$	C-type	hexagonal	hexagonal	hexagonal	hexagonal	hexagonal
$Y_{0.3}Gd_{0.7}InO_3$	C-type	C-type	hexagonal	hexagonal	hexagonal	hexagonal
$Y_{0.5}Gd_{0.5}InO_3$	C-type	C-type	hexagonal	hexagonal	hexagonal	hexagonal
$Y_{0.7}Gd_{0.3}InO_3$	C-type	C-type	C-type + hexagonal	hexagonal	hexagonal	hexagonal
$Y_{0.9}Gd_{0.1}InO_3$	C-type	C-type	C-type	C-type	C-type + hexagonal	hexagonal
$YInO_3$	C-type	C-type	C-type	C-type	C-type	hexagonal

and the strain increases with an increase in Gd^{3+} substitution (Figure S1, Supporting Information).

On heating the nominal compositions at 1100 °C, it was observed that the compositions $Y_{1-x}Gd_xInO_3$ ($0.0 \le x \le 0.7$) have transformed to the hexagonal modification. Further heat treatment at 1250 °C converted the rest of the nominal compositions also to the hexagonal form, i.e., $Y_{0.9}Gd_{0.1}InO_3$ and $YInO_3$ (Figure 1b). Thus at 1250 °C, the entire series $Y_{1-x}Gd_xInO_3$ ($0.0 \le x \le 1.0$) exists in the single-phasic hexagonal form. This aligns with the fact that both the end members are hexagonal, and hence complete solubility of Gd in $YInO_3$ or vice versa could be achieved. This temperature dependence of phase relations invokes a lot of interest here because as discussed in the Introduction, when r_A and r_B become comparable, the C-type or bixbyite phase of ABO_3 composition crystallizes. However here, the tolerance factor is much higher that that corresponding to the bixbyite-type phase (Table 1). The C-type to hexagonal and vice versa is a reconstructive phase transition.

dx.doi.org/10.1021/ic402085w | Inorg. Chem. 2013, 52, 13179−13187

Thus, it is obvious that the as-obtained C-type phase for these nominal compositions is the metastable phase, which on heating transforms to the hexagonal phase, the reported stable phase for the parents $YInO_3$ and $GdInO_3$. Thus, the stabilization of the metastable C-type phase for these nominal compositions can be attributed to the kinetic stability brought about by the nonequilibrium synthesis method adopted here, which brings about the randomization of all the cations, despite the ionic size difference, favoring the C-type configuration. The schematic structures for C-type and hexagonal modifications are depicted in Figure 2. Table 2 gives the phases observed for different nominal compositions at various temperatures. It may be inferred from Table 2 that the conversion temperature from metastable C-type to stable hexagonal phase is lowest (800 °C) for $GdInO_3$ and highest (1250 °C) for $YInO_3$ in the $Y_{1-x}Gd_xInO_3$ series. Thus, with an increase in the amount of Gd^{3+} ion in $YInO_3$, the transition temperature decreases. This can also be supported by calculating the tolerance factor, *t*, for various nominal compositions (Table 1). It is known[1] that the structure adopted by any particular ABO_3 composition depends upon the tolerance factor (*t*). The structure is cubic if *t* lies between 0.9 and 1. For *t* smaller than 0.9, it adopts the orthorhombic modification followed by various hexagonal forms, and finally when r_A and r_B are comparable, they adopt bixbyite or C-type modifications. The tolerance factor of $YInO_3$ is least among all the nominal compositions studied, and it increases with an increase in Gd^{3+} content. Hence, $YInO_3$ will have the least tendency to convert into the hexagonal modification among all the compositions in this series, and thus it requires a higher temperature for transition to the hexagonal modification, or, in other words, $YInO_3$ is most stable in the C-type modification among all compositions studied. This also explains the increase in transition temperature from C-type (bixbyite) modification to hexagonal modification with an increase in yttrium content.

Another interesting feature worth noticing here is that on subsequent substitution of Gd^{3+}, the peaks at $2\theta \approx 14°$ and $2\theta \approx 29°$ decrease in splitting. This indicates that the symmetry of the lattice is gradually increasing from $YInO_3$ to $GdInO_3$ even though both are the hexagonal phases. The presence of a small superstructure peak at ~33.5° (Figure 1b) throughout the series indicates that even though the system's symmetry is perhaps increasing with an increase in Gd^{3+} content, it still belongs to the low-symmetry hexagonal $P6_3cm$ space group.[11] The high-temperature, higher symmetry $P6_3mmc$ space group is centrosymmetric, unlike the low-temperature form, and the conversion between these two involves simple atomic displacements and hence is a displacive phase transition.

In order to investigate the detailed structural evolution on introduction of Gd^{3+} ions in the lattice, Rietveld refinement was performed on all the compositions in the series. The refinement results are summarized in Table 1. Typical refined patterns for $Y_{1-x}Gd_xInO_3$ (x = 0.0, 0.5, and 1.0) are shown in Figure 3. It is observed that the lattice parameters of the hexagonal phase increase with an increase in Gd^{3+} content. The trend can be explained by the increase in average cationic radii on substituting Gd^{3+} at the Y^{3+} site. The cationic radii of Gd^{3+} and Y^{3+} in 7-fold coordination are 1.0 and 0.96 Å, respectively.[15] The substitution of the smaller Y^{3+} by the larger Gd^{3+} causes an increase in both *a* (*b*) and *c* lattice parameters, which is expected due to the increase in average cationic size (Figure 4). However, the interesting observation is the extent of variation of bond lengths and/or lattice parameters of the hexagonal

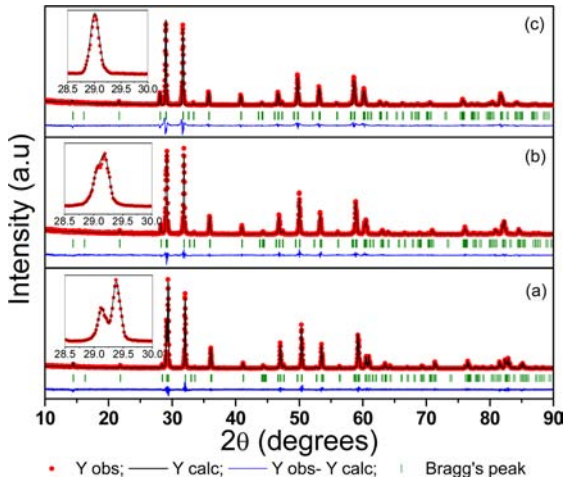

Figure 3. Typical fitted patterns of the representative nominal compositions (a) $YInO_3$, (b) $Y_{0.5}Gd_{0.5}InO_3$, and (c) $GdInO_3$.

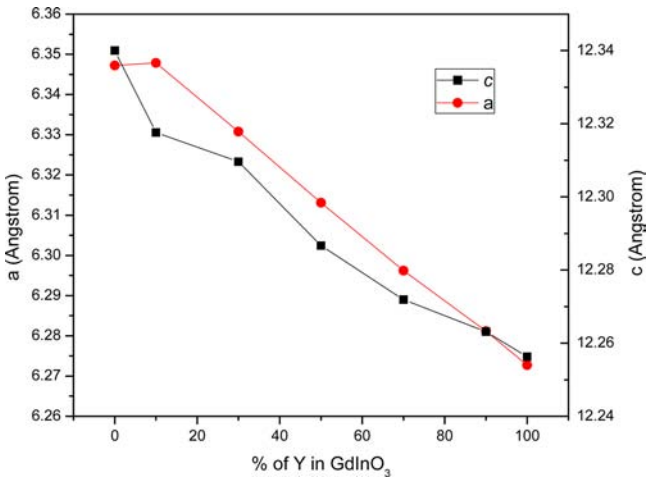

Figure 4. Lattice parameter variation of the nominal compositions in $Y_{1-x}Gd_xInO_3$ ($0.0 \le x \le 1.0$) with an increase in Gd^{3+} content.

phase on proceeding from pure $YInO_3$ to Gd^+-substituted $YInO_3$. For instance, a closer look at the trends in bond length variation of these compounds shows that in the InO_5 TBP polyhedron, the percentage increase of the apical bond lengths is almost half of the increase observed in planar bond lengths (Table 3). This trend in bond lengths is also reflected in the variation of "*a*" and "*c*" lattice parameters. This result differs from our previous study,[16] wherein the substitution of a heteroatom (Sc^{3+}) at the B-site of hexagonal $GdInO_3$ brought an increase in the *a* parameter and a decrease in the *c* parameter. If the hexagonal $P6_3cm$ structure is visualized, the A−O and B−O polyhedra are linked through a common oxygen along the *c*-axis. An increase in the A−O bond length (due to substitution of a larger Gd^{3+} in place of Y^{3+}) will create instability in the B−O bond by pushing them closer. This strain can be released in one of three ways: (a) the B−O bond along the *c*-axis also elongates, (b) the polyhedron tilts, i.e., the O−B−O angle changes, and (c) the axial/planar bonds increase. Since the polyhedral tilt does not change in this series and the increase in apical bond (*c* lattice parameter) is not much, the strain generated is primarily released by the relatively higher extent of expansion in the planar bonds. A schematic diagram depicting this is shown in Figure 5.

dx.doi.org/10.1021/ic402085w | *Inorg. Chem.* 2013, 52, 13179−13187

Table 3. Trend in In−O Bond Length (Å) Values (Apical and Planar) for the System $Y_{1-x}Gd_xInO_3$ ($0.0 \le x \le 1.0$)

	composition					
	$YInO_3$	$Y_{0.9}Gd_{0.1}InO_3$	$Y_{0.7}Gd_{0.3}InO_3$	$Y_{0.5}Gd_{0.5}InO_3$	$Y_{0.3}Gd_{0.7}InO_3$	$GdInO_3$
$In-O1_{apical}$	2.1210	2.1249	2.1266	2.1290	2.1333	2.1331
$In-O2_{apical}$	2.0994	2.1033	2.1050	2.1075	2.1117	2.1116
$In-O3_{planar}$	2.1177	2.1245	2.1295	2.1350	2.1414	2.1457
$In-O4_{planar}$	2.1104	2.1157	2.1222	2.1262	2.1326	2.1384
$In-O5_{planar}$	2.1108	2.1160	2.1226	2.1265	2.1329	2.1388

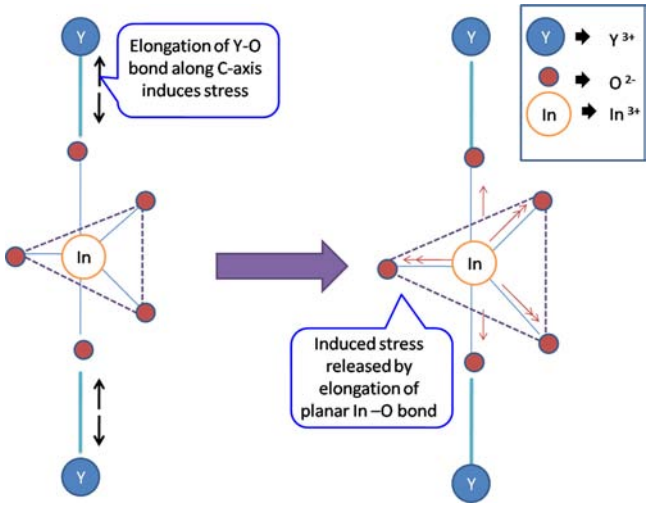

Figure 5. Schematics depicting the release of lattice strain on a larger Gd^{3+} introduction in the $YInO_3$ lattice by higher expansion in the *ab*-plane.

RAMAN SPECTROSCOPY

It has been well documented and known that Raman spectroscopy is a highly sensitive and simple laboratory-scale technique to detect local as well as subtle structural variations in materials. To further explore the local structure in the present series, all the nominal compositions were subjected to Raman spectroscopic studies.

There is only a single report[17] that shows the Raman spectrum of $YInO_3$ to the best of our knowledge. However, its crystal structure resembles $YMnO_3$ (both of these are $LuMnO_3$-type), which is a well-studied multiferroic system crystallizing in the $P6_3cm$ lattice. Hence, for the rest of the discussion, the Raman studies on $YMnO_3$ will be referred to for comparison. The elementary cell for this space group consists of six formula units. From the group theoretical analysis, it has been calculated that out of the total 60 phonon modes (10A1 + 5A2 + 10B1 + 5B2 + 15E1 + 15E2),[15] only 38 are Raman active, which are given by 9A1 + 14E1 + 15E2. Even though all these 38 modes are Raman active, all of them have not yet been reported at least for $YMnO_3$. As discussed in the previous section, the ferroelectricity of the $P6_3cm$ space group is attributed to the small tilting/distortion of InO_5 polyhedra from the *c*-axis. Because of a very small distortion being responsible for the electrical behavior, the Raman bands are weak, and hence many of them are usually not observed.

In the present study, the major Raman bands for $YInO_3$ are observed at 152, 207, 217, 226, 246.39, 297, 323.7, 361.9, 377.4, 431, 508, 520, 609, and 648 cm^{-1}. This is in reasonable agreement with that reported for $YMnO_3$ by Iliev et al.[18] in their exhaustive Raman studies on $YMnO_3$. They have also related the observed wave numbers to the atomic displacements involved. On comparing the Raman spectra of $YMnO_3$ and $YInO_3$ (since it has not been discussed in the literature), it is interesting to note that the Raman bands involving atomic displacements of apical oxygens (609, 238 cm^{-1}, etc.) show a distinct shift to lower wavenumber in the $YInO_3$ spectrum as compared to $YMnO_3$, whereas not much shift is observed in the modes involving planar oxygens (433, 297 cm^{-1}, etc.). This can be attributed to relatively longer In−O apical bonds as compared to Mn−O bonds. This has been shown by Smith et al.,[19] on comparing the trigonal bipyramidal coordination of Mn and In in respective compounds, that planar bond lengths do not change much, and it is the apical B−O bonds that change on substituting Mn for In in the $Y(In,Mn)O_3$ series.

The Raman spectra of various nominal compositions in the $Y_{1-x}Gd_xInO_3$ ($0.0 \le x \le 1.0$) system from pure $YInO_3$ to pure $GdInO_3$ are depicted in Figure 6. A careful analysis of the

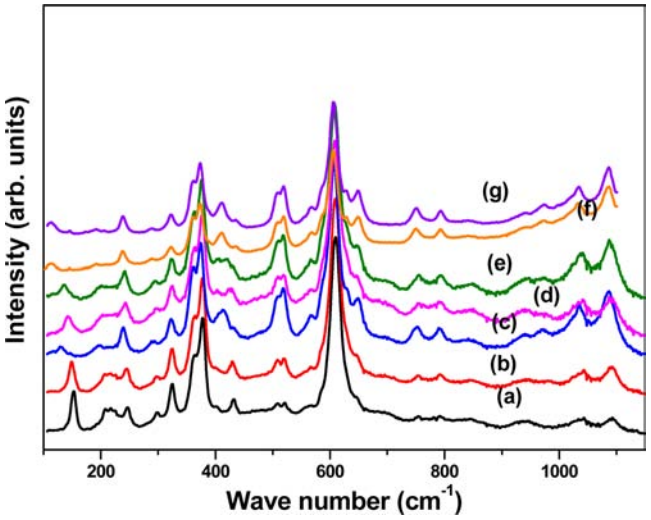

Figure 6. Raman spectrum for different nominal compositions in the series $Y_{1-x}Gd_xInO_3$ ($0.0 \le x \le 1.0$), namely, (a) $YInO_3$, (b) $Y_{0.9}Gd_{0.1}InO_3$, (c) $Y_{0.7}Gd_{0.3}InO_3$, (d) $Y_{0.5}Gd_{0.5}InO_3$, (e) $Y_{0.3}Gd_{0.7}InO_3$, (f) $Y_{0.1}Gd_{0.9}InO_3$, and (g) $GdInO_3$.

Raman spectra reported for different nominal compositions in $Y_{1-x}Gd_xInO_3$ reveals that there is a general trend in the Raman spectra being shifted to lower wavenumber; that is, softening of Raman modes is taking place (Figure 6). It has been reported that the Raman frequencies depend significantly on unit cell volume. On substituting Gd^{3+} for Y^{3+}, as is reported in Table 1, the cell parameters (*a* (*b*) and *c*) increase, and hence the unit cell volume is increasing, which implies that the Raman bands should be red-shifted, as is also observed. Also, the various Raman bands show broadening with an increase in the amount of Gd^{3+} (in $YInO_3$) or vice versa due to the disorder created in the lattice at the A-site owing to the presence of two cations (Gd^{3+} and Y^{3+}). With a change in nominal composition, the

dx.doi.org/10.1021/ic402085w | Inorg. Chem. 2013, 52, 13179−13187

occupancy at the A-site changes. The fact that Gd−O and Y−O bonds will have different strength will influence their vibration frequencies, and hence a spread in frequency would be observed. There have been similar examples in the literature,[20] wherein the substitution leads to the broadening of the Raman bands. It is further supported by the fact that the broadening increases with an increase in Gd^{3+} substitution, reaches a maximum at 50 mol % substitution, where there should be maximum randomization, and then successively narrows as the amount of Gd^{3+} increases.

A striking observation in the Raman spectrum of these indates is relatively higher intensities of the 377 and 612 cm^{-1} bands, belonging to A_1 and E_1 symmetries, compared to other bands of the same symmetry. The same has been observed by Iliev et al.[18] and Fukumara et al.[21] for $YMnO_3$ and has been ascribed to the fact that each phonon mode of the noncentrosymmetric $P6_3cm$ space group has a zone boundary counterpart mode involving similar atomic motions in the $P6_3mmc$ space group. Since the distortion that brings about the transition from $P6_3cm$ to $P6_3mmc$ is very small, A_1 and E_1 modes, which correspond to the Raman-active A_{1g} and E_{1g} modes in P63/*mmc* should give rise to much stronger lines as compared to the Raman-inactive modes in *P*63/*mmc*. Iliev et al.[18] have carried out a detailed study and have correlated various bands in the $YMnO_3$ spectrum to the respective atomic displacements. A comparison with their study and a careful observation of the Raman spectra obtained in the present study show that the modes involving vibrations due to planar oxygens (e.g., 152, 246, 437 cm^{-1}) show greater red shift as compared to the modes involving apical oxygens (e.g., 610, 377 cm^{-1}) with an increase in the amount of Gd^{3+}. This is in concurrence with the X-ray diffraction studies, wherein it could be shown by detailed structural refinements that the changes observed in planar bonds are much greater than those observed in apical bonds on successive Gd^{3+} substitution.

The frequencies of various modes observed in the Raman spectra of different nominal compositions are plotted with respect to the composition and are depicted in Figure 7(a and b). It is quite obvious from these plots that there is a distinct change in the slope at the nominal composition $Y_{0.3}Gd_{0.7}InO_3$. The same trend could be observed for more than one mode as shown. This indicates that even though in the present series, by XRD studies, the structural change is observed to be gradual with no concomitant change in the space group, there is a noticeable structural change occurring in the system at 70 mol % Gd^{3+} substitution. This shows the importance of Raman spectroscopy to detect the subtle changes in the lattice that cannot be observed by general macroscopic lab-scale structure determination techniques based on diffraction.

ELECTRICAL STUDIES

All the nominal compositions prepared in the present series were subjected to detailed PE studies (electric field dependent polarization), which revealed a very interesting trend in the PE behavior of the nominal compositions with a change in composition (Gd^{3+}/Y^{3+} content). It was observed that $YInO_3$ showed a ferroelectric PE loop at room temperature, though a little lossy, as depicted in Figure 8. It may be noted that the hexagonal rare-earth indates and managanites (e.g., $YMnO_3$) are not conventional ferroelectrics, and this may be the reason that ferroelectrics based on d^0 systems such as $BaTiO_3$ show superior PE characteristics. For $YInO_3$, at the field gradient of 5 kV/cm, the P_{max} of 0.02 $\mu C/cm^2$ was observed. It is interesting

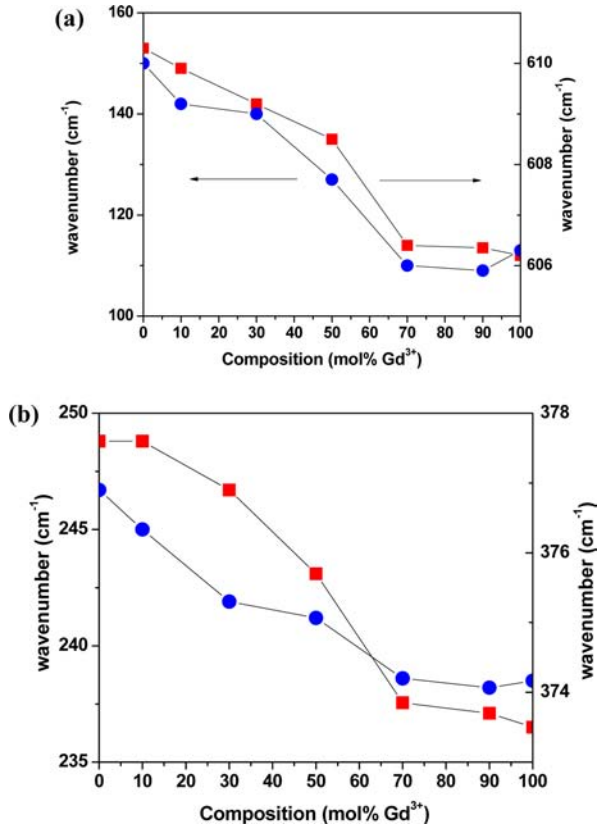

Figure 7. Variation of frequencies of various modes in Raman spectra with composition in $Y_{1-x}Gd_xInO_3$ ($0.0 \leq x \leq 1.0$).

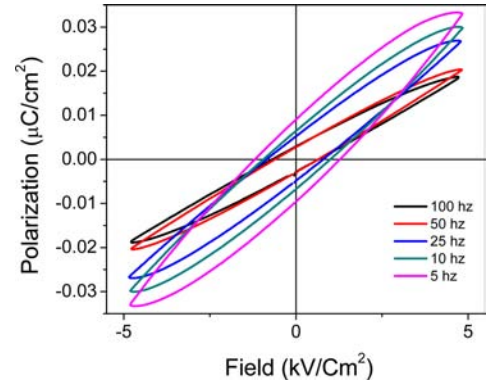

Figure 8. Polarization−electric field characteristics of ferroelectric $YInO_3$ as a function of frequency.

to note that with 10 mol % Gd^{3+} substitution there is a significant change in P_{max}, which becomes 0.045 $\mu C/cm^2$. There is a concomitant change in P_r (remanence) and E_c (coercivity) as well, which increase by almost 3 times (Figure 9). This may be attributed to the presence of different cations at the A-site, which might add to better retention of charge in the sample. However, the leakage current also increases simultaneously. With further Gd^{3+} substitution (30 and 50 mol %), there is not much change in the PE characteristics however. Curiously, the PE loop again narrows significantly on increasing the Gd^{3+} content to 70 mol %. In fact, the PE characteristic of the nominal composition $Y_{0.7}Gd_{0.3}InO_3$ is very slim with much less remanence. It should also be mentioned here that this particular composition had the least leakage current in the present series, which is an order of magnitude less than pure $YInO_3$. At the

dx.doi.org/10.1021/ic402085w | Inorg. Chem. 2013, 52, 13179−13187

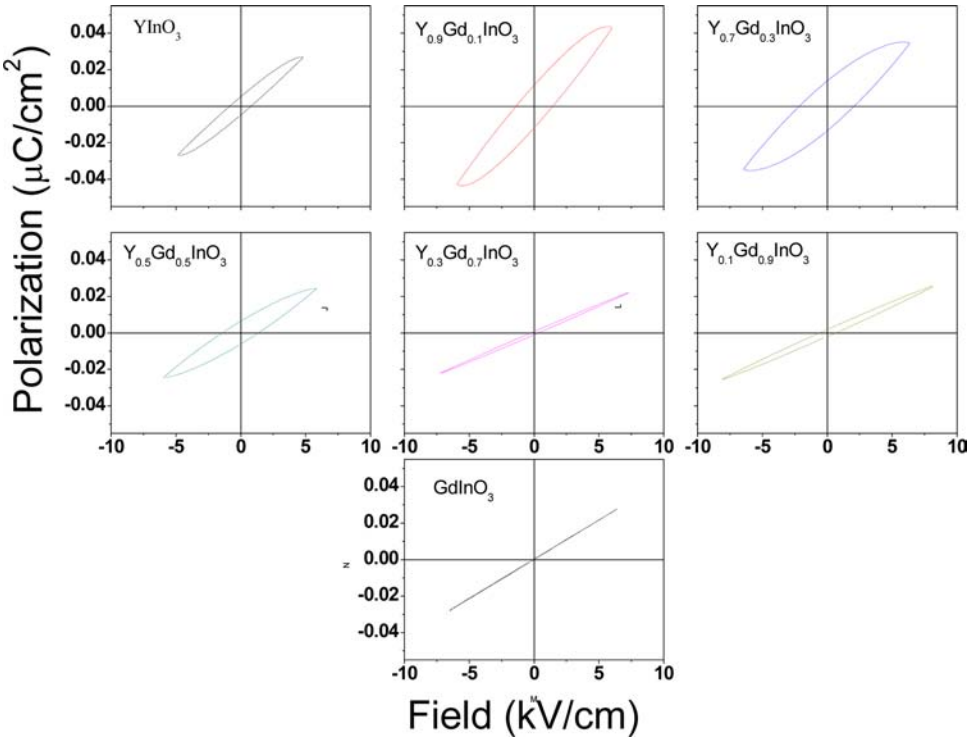

Figure 9. Polarization−electric field characteristics of various nominal compositions in $Y_{1-x}Gd_xInO_3$ ($0.0 \leq x \leq 1.0$).

field gradient of 0.4 kV/cm, whereas the leakage current varied from 1×10^{-3} to 3×10^{-3} μA/cm^2, it was found to be 0.1×10^{-3} μA/cm^2 for this particular composition. The PE loop belonging to $GdInO_3$ is more indicative of the paraelectric compound with almost a straight line behavior (Figure 9).

Detailed dielectric studies were performed to substantiate the PE studies. The temperature dependence of the dielectric constant (relative permittivity) ε' at several frequencies is shown in Figure 10 for all samples. It has been reported in the literature that T_C for $YInO_3$ is ~560 °C.[22] Since in the present studies measurements have been performed only until 300 °C, no ferroelectric to paraelectric transition peak could be observed in the permittivity−temperature graph for $YInO_3$. Within the temperature range investigated, for samples with $0 \leq x \leq 0.7$, the relative permittivity is nearly unchanged at lower temperatures, but increases rapidly at temperatures above 200 °C. It is observed from these graphs that from $x = 0.7$ onward there is an appearance of a broad and weak peak near 100 °C. The peak shows a frequency dependence that is significant for $x = 0.7$, as is observed from Figure 10. The PE loop for this composition is a very narrow loop, indicating relaxor behavior. However, on close examination of the ε' vs T curve in the temperature range 80−150 °C, it is very difficult to conclude about the peaking behavior, since the variation in dielectric constant with temperature appears more like a step. Hence, it cannot be conclusively called a relaxor behavior. With these studies alone, it would be more appropriate to explain them as defect-mediated relaxations occurring in this temperature range. The maximum value of permittivity (at 100 Hz and 300 °C) increases from about 40 for $x = 0.0$ ($GdInO_3$) to about 150 for $x = 0.5$, before decreasing to around 45 in the sample with $x = 1.0$ ($YInO_3$). The corresponding values of the dielectric loss tangent, tan δ, which is the ratio of the imaginary part to the real part of the relative permittivity, are 0.38 for $x = 0.0$, 1.2 for $x = 0.5$, and about 0.6 for $x = 1.0$, respectively. The rapid increase in relative permittivity may be attributed to interfacial polarization at the electrodes as well as due to a conductivity contribution, possibly due to defects in the crystalline structure. Thus, it can be deduced that a peaking effect in the relative permittivity is brought about by the changes in the defect concentration as the doping concentration x is changed.

The electrical studies thus show a transition from ferroelectric behavior to paraelectric behavior with an increase in concentration of Gd^{3+}. However, electrical studies throw light on an important factor. Even though the overall structural lattice retains the space group ($P6_3cm$), the subtle distortions in the structure of solid solutions (instrumental in controlling the electrical behavior) apparently are of two types in this system. The nominal compositions from $x = 0$ to $x = 0.5$ fall under one category with approximately similar PE behavior and leakage characteristics, whereas the nominal compositions from $x = 0.7$ to $x = 1.0$ fall into a second category. This is supported by the nature of the variation of ε' with temperature for these compositions. This is also corroborated by the detailed Raman analysis, wherein a distinct change in the slope of frequencies of various modes could be observed at $x = 0.7$. This structural change needs to be thoroughly studied by detailed local structure analysis techniques such as EXAFS, as it could be of importance in yielding superior electrical materials. Similar studies are presently under way. Concerning the electrical behavior also, it would be worthwhile mentioning here that there have been detailed reports on $YMnO_3$ wherein, by extensive theoretical and statistical experimental analyses, it has been shown that even within the $P6_3cm$ space group there should be the existence of a nonferroelectric form of $YMnO_3$.[23,24] This has been supported by the fact that in the case of $YMnO_3$ T_{FE} (ferro to para) and T_{PT} (phase transition) do not coincide. The ferroelectric to paraelectric $P6_3cm$ is said to be brought about by a displacement of the oxygen and manganese ions within the 5-fold coordination polyhedron of

dx.doi.org/10.1021/ic402085w | Inorg. Chem. 2013, 52, 13179−13187

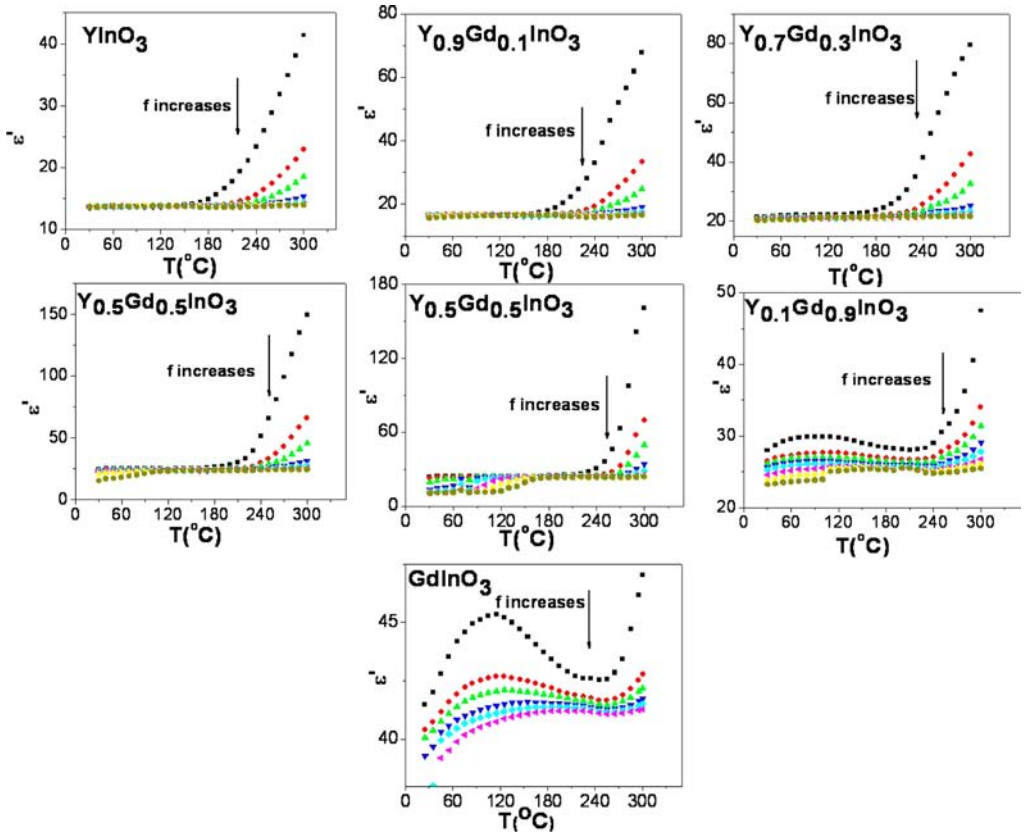

Figure 10. Temperature dependence of the dielectric constant (relative permittivity) ε' at several frequencies for the $Y_{1-x}Gd_xInO_3$ ($0.0 \leq x \leq 1.0$) system.

Mn without tilting the trigonal bipyramid. We assume that substituting Gd^{3+} for Y^{3+} in $Y_{1-x}Gd_xInO_3$ indeed brings about this displacement in the lattice without changing the space group. However, conclusive evidence can only be provided by detailed theoretical and experimental studies on this system similar to $YMnO_3$.[23]

Previously, a relaxor behavior could be reported in a hexagonal doped $GdIn_{1-x}Sc_xO_3$ ($0.0 \leq x \leq 1.0$)[16] system (which involved doping at the B-site). On comparing the present work on $Y_{1-x}Gd_xInO_3$ ($0.0 \leq x \leq 1.0$) with $GdIn_{1-x}Sc_xO_3$ ($0.0 \leq x \leq 1.0$),[16] it becomes clear that, even in the hexagonal regime, a tailoring of electrical behavior is more influenced by B-site substitution than by A-site substitution. As is discussed previously, the occurrence of geometric ferroelectricity in these hexagonal rare-earth indates is controlled by alternating A−O bond lengths and the tilt of InO_5 polyhedra. The A-site substitution, although affecting the average A−O bond length, does not influences the tilt of InO_5 polyhedra. It seems plausible here to conclude that to control/tailor the tilt of the InO_5 trigonal bipyramid, it is more important to tailor the B-site occupant.

CONCLUSIONS

The $Y_{1-x}Gd_xInO_3$ ($0.0 \leq x \leq 1.0$) complex oxides were explored by structural and electrical investigations. The phase relation was observed to be single phasic in the hexagonal $P6_3cm$ space group at 1250 °C. The metastable C-type modification in the $Y_{1-x}Gd_xInO_3$ system could be stabilized, which converted to a stable hexagonal polymorph with the transition temperature increasing with an increase in Y-content. The increase in the *c*-lattice parameter was half of that observed in the *a*,*b*-plane on Gd^{3+} substitution. Even though XRD studies revealed a hexagonal $P6_3cm$ space group throughout the composition range, Raman studies indicated a subtle structural variation in the lattice of 70 mol % Gd substituted $YInO_3$ onward. The PE studies showed a ferroelectric hysteresis loop for $YInO_3$, which improves slightly with 10 mol % Gd substitution and then deteriorates. $GdInO_3$ was observed to show a paraelectric behavior. The dielectric ε' vs T curve in the temperature range 80−150 °C also pointed toward a subtle structural shift in the lattice, thus supporting the Raman studies. As the hexagonal rare-earth indates are emerging as an important class of geometric ferroelectrics, where structural tunability of electrical properties is a wide open area of research, the present study shows that whereas structurally A-site doping may reveal interesting features for materials scientists to investigate, these do not result in drastic changes in electrical properties.

ASSOCIATED CONTENT

Supporting Information

This material is available free of charge via the Internet at http://pubs.acs.org.

AUTHOR INFORMATION

Corresponding Authors

*E-mail: vinita@barc.gov.in. Phone: 0091-22-25595330. Fax: 0091-22-25505151.

*E-mail: aktyagi@barc.gov.in.

Notes

The authors declare no competing financial interest.

■ ACKNOWLEDGMENTS

The Department of Atomic Energy's Science Research Council (DAE-SRC) is acknowledged for supporting this work via sanction number no. 2010/21/9-BRNS/2025 dated 7−12−2010.

■ REFERENCES

(1) Giaquinta, D. M.; zur Loye, H.-C. *Chem. Mater.* **1994**, *6*, 365.
(2) Katsufuji, T.; Mori, S.; Masaki, M.; Moritomo, Y.; Yamamoto, N.; Takagi, H. *Phys. Rev. B* **2001**, *64*, 104419.
(3) Yakel, H.; Koehler, W.; Bertaut, E.; Forrat, F. *Acta Crystallogr.* **1963**, *16*, 957.
(4) Van Aken, B. B.; Meetsma, A.; Palstra, T. M. *Acta Crystallogr.* **2001**, *230*, c57.
(5) Ismailzade, I. G.; Kizhaev, S. A. *Sov. Phys. Solid State* **1965**, *7*, 236.
(6) Floros, N.; Rijssenbeek, J. T.; Martinson, A. B.; Poeppelmeier, K. R. *Solid State Sci.* **2002**, *4*, 1495.
(7) Vander Griend, D. A.; Malo, S.; Wang, K. T.; Poeppelmeier, K. R. *J. Am. Chem. Soc.* **2000**, *122*, 7308.
(8) Malo, S.; Maignan, A.; Marinl, S.; Hervieu, M.; Poeppelmeier, K. R.; Raveau, B. *Solid State Sci.* **2005**, *7*, 1492.
(9) Van Aken, B. B.; Palstra, T. T. M.; Filippetti, A.; Spaldin, N. A. *Nat. Mater.* **2004**, *3*, 164.
(10) Pistorius, C. W. F. T.; Kruger, G. J. *J. Inorg. Nucl. Chem.* **1976**, *38*, 1471.
(11) Tohei, T.; Moriwake, H.; Murata, H.; Kuwabara, A.; Hashimoto, R.; Yamamoto, T.; Tanaka, I. *Phy. Rev. B* **2009**, *79*, 144125.
(12) Sleight, A. W. *Prog. Solid Sate Chem.* **2009**, *37*, 251.
(13) Smith, A. E.; Mizoguchi, H.; Delaney, K.; Spaldin, N. A.; Sleight, A. W.; Subramanian, M. A. *J. Am. Chem. Soc.* **2009**, *131*, 17084.
(14) Rodriguez-Carvajal, J. *Fullprof 2000, a Program for Rietveld, Profile Matching and Integrated Intensity Refinements for X-ray and Neutron Data*, Version 1.6; Laboratoire Leon Brillouin, Gif sur Yvette: France, 2000.
(15) Shannon, R. D. *Acta Crystallogr.* **1976**, *A32*, 751.
(16) Grover, V.; Shukla, R.; Jain, D.; Deshpande, S. K.; Arya, A.; Pillai, C. G. S.; Tyagi, A. K. *Chem. Mater.* **2012**, *24*, 2186.
(17) Arai, N.; Saito, N.; Nishiyama, H.; Shimodaira, Y.; Kobayashi, H.; Inoue, Y.; Sato, K. *Chem. Lett.* **2008**, *37*, 46.
(18) Iliev, M. N.; Lee, H. G.; Popov, V. N.; Abrashev, M. V.; Hamed, A.; Meng, R. L.; Chu, C. W. *Phys. Rev. B* **1997**, *56*, 2488.
(19) Smith, A. E.; Mizoguchi, H.; Delaney, K.; Spaldin, N. A.; Sleight, A. W.; Subramanian, M. A. *J. Am. Chem. Soc.* **2009**, *131*, 17084.
(20) Banerji, A.; Grover, V.; Sathe, V.; Deb, S. K.; Tyagi, A. K. *Solid State Commun.* **2009**, *149*, 1689.
(21) Fukumura, H.; Matsui, S.; Harima, H.; Kisoda, K.; Takahashi, T.; Yoshimura, T.; Fujimura, N. *J. Phys.: Condens. Matter* **2007**, *19*, 365239.
(22) Abrahams, S. C. *Acta Crystallogr.* **2001**, *B57*, 485.
(23) Lonkai, Th.; Tomuta, D. G.; Amann, U.; Ihringer, J.; Hendrikx, R. W. A.; Tobbens, D. M.; Mydosh, J. A. *Phys. Rev. B* **1997**, *69*, 134108.
(24) Nenert, G.; Pollet, M.; Marinel, S.; Blake, G. R.; Meetsma, A.; Palstra, T. T. M. *J. Phys.: Condens. Matter* **2007**, *19*, 466212.